Constraining the geometry and properties of the upper crust by means of potential field anomalies: a case study from the Cameros Basin (North Spain)

P. del Río[1], A. Casas[1], J. Villalaín[2], T. Mochales[1], R. Soto[3], B. Oliva-Urcia[4]

[1]Departamento de Ciencias de la Tierra. Universidad de Zaragoza. C/Pedro Cerbuna, 12, 50009 Zaragoza (Spain)

[2]Departamento de Física. Universidad de Burgos. Avda. de Cantabria s/n 09006 Burgos (Spain)

[3]Instituto Geológico y Minero de España. Oficina de Proyectos de Zaragoza. C/Manuel Lasala 44 9B 50006 Zaragoza (Spain)

[4]Instituto Pirenaico de Ecología. IPE-CSIC, Avda. Montañana 1005, 50059 Zaragoza (Spain)

Abstract

Outstanding potential field anomalies (gravimetric and magnetic) in the Cameros Basin (N Spain) follow a WNW-ESE trend, parallel to the geological structures resulting from Mesozoic extension and Tertiary basin inversion. The positive Bouguer anomaly (15 mGal) is interpreted in this work as the result of a strong contrast between the density of Tertiary rocks of the foreland basin and the Paleozoic and Mesozoic rocks, combined with crustal thickening in the Iberian Chain with respect to the Ebro Basin. The dipolar, normal magnetic anomaly, slightly shifted to the south with respect to the relative maximum of the Bouguer anomaly, can be interpreted as related to volcanic rocks within the basement, which are linked to Triassic rifting as witnessed by outcrops of

basalts along the basin margins. An exhaustive analysis of properties of rocks (density, magnetic susceptibility and remanence) and basin geometry from other sources (seismic reflection profiles) allow to constrain variations in crustal thickness and the location of large-scale basement faults.

Keywords: gravity, magnetics, modeling, sedimentary basin, Iberian plate, Cameros Basin

Introduction

Gravity and magnetic surveys are powerful tools to constrain the subsurface geometry of geological bodies. Their relative low cost- and time-efficiency with respect to other methods and the possibility of covering wide areas and imaging the 3-D shape of the subsurface are the main advantages of these kind of surveys. The shape and intensity of anomalies are two key factors to constrain the shape of the causative bodies, together with the properties of the materials involved.

The Iberian Peninsula shows well-defined potential field anomalies related to the existence of igneous or mantelic bodies (Casas et al., 1997; Aller et al., 1997; Aranguren et al., 2003; Ayarza and Martínez-Catalán, 2007), changes in crustal thickness (Salas and Casas, 1993; Guimerà et al., 1996; Rey-Moral et al., 2003, De Vicente, 2004 and references therein, Gómez-Ortiz et al., 2005) and other minor anomalies related to Tertiary basins (Pedrera et al., 2010), diapirs (Pinto et al., 2005; Santolaria et al., 2012) and other geological structures (Casas et al., 2000; Ruiz-Constán et al., 2009). The Iberian chain, located in the North-Eastern part of the Iberian

Peninsula is characterized by strong negative Bouguer anomalies associated with crustal thicknening (Salas and Casas, 1993; Mezcua et al., 1996 Guimerà et al., 1996) and local dipolar (normal and reverse) magnetic anomalies (Instituto Geográfico Nacional, 2001), whose origin has not been elucidated in many cases and in others is related to Permian or Triassic volcanism (Calvín et al., 2012).

The main objective of this work is to determine the origin of the gravimetric and magnetic anomalies existing in the Cameros Basin (Fig. 1), the westernmost sector of the Iberian Chain and the area of strongest subsidence during the Mesozoic in the inner part of the Iberian plate. To reach this goal, we profit from the well-constrained geometry (mainly by means of seismic reflection profiles and surface geology) of shallow geological structures within the Basin. The used methodology includes: i) measuring the magnetic and gravity fields along profiles perpendicular to the main structures by means of detailed surveys, ii) measurements of properties (magnetic susceptibility and remanence, and density) of rocks cropping out at surface and iii) 2.5D modeling of the potential field anomalies obtained.

Geological setting

The Cameros Basin is one of the most important Mesozoic features within the Iberian Peninsula (Fig. 1.A) because of its 8 km thick sedimentary infill during the Late Jurassic-Early Cretaceous rifting stage (Guiraud and Séguret, 1984; Casas-Sainz and Gil-Imaz, 1997; Casas et al., 2009). The extensional basin was totally inverted during the Tertiary compressional stage (Eocene-Miocene, Muñoz-Jiménez and Casas-Sainz, 1997). The good outcrop conditions and the availability of seismic sections west of the

studied area (Fig. 2) make possible to constrain the present-day geometry down to 5 km depth.

During Mesozoic times the Cameros Basin was mostly a continental sedimentary basin originated by the intracontinental rift related to the opening of the North Atlantic Ocean and the Bay of Biscay. Its Triassic-Early Jurassic evolution was particularly important because large volumes of volcanic rocks were emplaced within Upper Triassic mudstones (Lago et al., 1996, 1998; Fig. 1D), probably indicating an incipient plate margin (Salas and Casas, 1993). Outcrops of basaltic sills show a NW-SE orientation parallel to the main structures. This volcanic episode represents an alkaline magmatism, which is contemporary with the beginning of the rifting in the western Tethys (Lago et al., 1996).

The Early Cretaceous was the most important rifting stage in the Cameros Basin, with up to 8 km of syn-rift deposits in the centre of the basin. Rifting was linked to normal faulting in the northern basin border and secondary faults in the south. The Albian marks the end of the large extension, leading to a post-rift stage marked by continental and then marine sedimentation (Muñoz et al., 1997). Basin inversion during the Tertiary resulted in the displacement of the whole Mesozoic basin towards the North (Casas-Sainz, 1993) over the Tertiary molasse of the Rioja Trough, with average displacements of 25 (horizontal) and 4 (vertical) km (Muñoz-Jiménez and Casas-Sainz, 1997).

The main stratigraphic units that crop out in the studied area show similar properties, within the range established for sedimentary rocks. The Paleozoic is constituted by Cambrian-Ordovician sandstones and mudstones with interspersed dolostones and

igneous rocks. The Triassic rocks include sandstones, limestones (a few meters in thickness), clays and gypsum (Keuper facies). The Marine Jurassic is about 1,000 m thick and is mainly formed by marine limestones. The syn-rift sequence (Tithonian-Early Albian) is formed mainly by continental sediments, divided in 5 lithostratigraphic groups (Tischer, 1966): Tera (siltstones and conglomerates), Oncala (lacustrine carbonates and siltstones), Urbión (fluvial sandstones and siltstones), Enciso (limestones and siltones) and Oliván (fluvial sandstones and siltstones). The post rift sequence is constituted by sands and marine sandstones that represent the Cenomanian transgression. The syn-compressional units of Tertiary age are conglomerates, sandstones, shales and lesser proportions of limestones and gypsum in the basin centre.

The structure of the Cameros Basin was controlled by inherited Variscan structures (Arthaud and Matte, 1975) reactivated during Mesozoic rifting. The main extensional structure was a listric fault located at the northen margin of the basin which controlled the syn-rift sedimentation (Casas-Sainz, 1993; Casas-Sainz and Gil-Imaz, 1997). During Eocene-Oligocene, the compressional tectonics produced the tectonic inversion of the basin, and exhumation of the deep (more than 4 km) sequences. A new thrust plane was formed (North Cameros Thrust; Fig. 1.C) producing the displacement of the hanging-wall 30 km over the Tertiary sediments of the Ebro basin. Main folds that control the geometry of the range are the North Cameros syncline and the Oncala anticline (Fig. 2).

Methodology

From the anomaly maps of the Iberian Peninsula (Mezcua et al., 1996; Instituto Geográfico Nacional, 2001; see also Rey-Moral et al., 2003) it can be seen that the

Bouguer, gravimetric and magnetic anomalies show a WNW-ESE trend, parallel to the dominant structural trend in the western sector of the Iberian Chain (Fig. 1). To characterize these anomalies, a detailed geophysical survey was carried out along a transect across the Iberian Chain, measuring both the gravimetric and magnetic field. For the gravimetric measurements, a Burris ZLS gravity meter was used, with an instrumental derive of 0 mGal in the period of the survey and a precision of 0.01 mGal. 75 new gravity stations were taken, spaced 1 km in average, and elevations were determined from geodetic benchmarks in 1:10,000 scale maps and a barometric altimeter with precision of ±0.5 m. This procedure enabled to estimate error margins of ±0.15 mGal during the gravity field exploration.

Elevation, Bouguer (with a reduction density of 2,700 kgm^{-3}, matching the average density of rocks in the Cameros Basin), latitude and topographic corrections (up to 20 km) were applied to all gravity values. A modeling program for 2.5D interpretation of gravity data (GravMag, from the British Geological Survey) was used for defining the geometry of bodies in cross-section. Both gravity and magnetic anomalies were projected in the same section, with a N015E orientation (Fig. 2).

The magnetic field was recorded with a rover magnetometer based on the Overhauser effect (GSM-19, GEM systems) with an accuracy of 0.1 nT, along a continuous profile, with more than 100,000 individual measurements taken. A base station was placed to account for diurnal corrections with a proton magnetometer (PGM-01 Czech Republic). Diurnal, altitude, latitude and regional corrections and filtering of local anomalies linked to human activity were applied. Data were averaged every 100 m to define the magnetic profile.

Density, magnetic susceptibility and magnetic remanence were estimated from about 1,000 samples in the different units cropping out in the Cameros Basin, Rioja Trough and adjacent areas. Densities were measured using the weight of the sample in air and water. For measuring the magnetic susceptibility data a KLY-3S Kappabridge (AGICO Inc., Czech Republic) in the University of Zaragoza was used in hand samples. Magnetic remanence was measured at the Paleomagnetics laboratory of the University of Burgos by means of a 2G-755 (Noise level 5×10^{-12} Am^{-1}) magnetometer. The database for the properties of rocks was completed with susceptibility data obtained from other works (Lasanta et al., 2011) in particular units of the Cameros Basin.

Results

Characterization of gravimetric and magnetic anomalies

The positive magnetic anomaly over the Cameros Basin shows a wavelength of 7 km and an amplitude of about 32 nT. The subsequent, northerly-switched negative anomaly shows a wavelength of 8 km and an amplitude of 29 nT (Fig. 1B). The Bouguer anomaly in this area shows a relative maximum, with a WNW-ESE oriented maximum showing a wavelength of 27 km, and an amplitude of about 30 mGal (Fig. 1C). Further south, a relative minimum of the Bouguer anomaly in the Almazán basin also shows a WNW-ESE trend (Rey-Moral et al., 1999; 2004). There is a difference in the location of the magnetic and gravimetric anomalies, being the axis of the dipole of the magnetic anomaly located slightly southward of the relative maximum of the Bouguer anomaly.

In the detailed profiles carried out in this work at the topographic level, the shape of the anomalies is better defined. The relative maximum of the Bouguer anomaly shows a clear asymmetry (Fig. 2), with a steeper slope in the norther sector, at the contact between the Rioja Trough and the Cameros Basin, and a gentler slope on the southern side, coinciding with the location of the Oncala anticline and connecting with the large negative anomaly in the central part of the Iberian Chain (Rey-Moral et al., 2003; De Vicente et al., 2004). The magnetic anomaly is characterised by a normal dipole with a tight positive part and a gentler negative one. This anomaly is centred in the southern slope of the relative maximum of the Bouguer anomaly (Fig. 2).

Properties of rocks

More than 1,500 samples of rocks about 11 cm^3 in volume were used to obtain statistically representative means of magnetic properties and density of the involved units (Fig. 3). The density values obtained in our measurements range between 2,500 and 2,800 kgm^{-3}. The lower density values correspond to the Tertiary deposits of the Rioja Trough and the Almazán Basin (average 2,500 kgm^{-3}), with a very (small) variability in spite of the strong differences in lithology (gypsum, shales, sandstones). The Palaeozoic and the Lower Cretaceous units show similar averages (2,700 kgm^{-3}) and variability of density, although within the Cretaceous units, differences can be established according to their position within the stratigraphic log (Fig. 3) and their content in pyrite, since pyrite-rich units show densities between 2,800 and 3,100 kgm^{-3}. The Triassic sandstones and shales and Jurassic limestones show typical values for these rock types, although their relevance is lower in terms of surface in the cross-sections (Fig. 3).

The results of the magnetic susceptibility measurements for the sedimentary rocks in the Cameros Basin show a wide range between negative values (dominance of the diamagnetic fraction in the susceptibility) and more 300×10^{-6} (S.I. units) (dominance of para- and ferromagnetic minerals in the susceptibility), with some samples showing values one order of magnitude higher due to the presence of iron oxides. Average for Palaeozoic rocks are about 200×10^{-6} (S.I. units) and for Mesozoic rocks of different units between 50 and 300×10^{-6} (S.I. units) (Fig. 3). The Tertiary rocks show considerably lower values (average 40×10^{-6} S.I. units) and Triassic basalts cropping out in the northern basin border are on the order of ($4{,}500\times10^{-6}$ S.I. units). Magnetic remanence indicates Koenigsberger ratios (Q) usually lower than 1 for most of the measured samples [Q = NRM/ (k×H); H=40A/m].

Modeling. Interpretation of potential field anomalies

Two models were performed in order to explain the potential field anomalies studied (Fig. 4). In the first one, the whole Cameros Basin is considered as an only body and therefore differences in properties between the different stratigraphic units are not considered. In the second model the input geometry is more detailed, thus allowing for differences in the inner part of the basin to be shown. The geometry of the syn-rift units in the Cameros Basin is well known, based on seismic profiles and outcrop observations (Casas-Sainz and Gil-Imaz, 1997, Muñoz-Jiménez and Casas-Sainz, 1997; Casas et al., 2009), and properties can be reasonably well constrained from the data obtained. Values for the lower crust and the mantle are the commonly used for the Iberian plate (Salas and Casas, 1993; De Vicente et al., 2004). The limit between the upper and middle crust

is located around 10 km, as assumed in other models in this sector of the Iberian Chain (Rey-Moral et al., 2000; De Vicente et al., 2009). The inputs for the model are shown in table 1.

Using these properties, the gravimetric profile approaches the observed values. The abrupt fall in the Bouguer anomaly in the northern sector can be explained by differences in density between the Mesozoic and the Tertiary and the important thickness (between 4 and 5 km) of Tertiary deposits. Some of the irregularities within the Rioja Trough cannot be explained by this simple model, and other values of density in the materials below (existence of anhydrite, limestones, etc) could be responsible for relative gravimetric maxima in this area. The southern half of the gravimetric anomaly can be partly explained by differences in crustal thickness linked to the regional anomaly associated with the Iberian Chain (De Vicente et al., 2004). To account for part of the shape of this curve in the detailed model, a lower density must be considered for the Oncala Group, according to its actual properties (Fig. 4).

Conversely, the magnetic anomaly located in the southern part of the Cameros Basin cannot be explained using the properties (susceptibility and remanence) obtained for most of the basement and cover rocks, and therefore the possibility of a high susceptibility body beneath the positive magnetic anomaly must be considered. The existence of Triassic intrusions all along the northern border of the Cameros Basin (Fig. 1.D) provides a possible source for the magnetic anomaly. Susceptibility of this body should range within $30\text{-}60\times10^{-3}$ S.I. and its location is constrained to the northern limb of the Oncala anticline. This dyke of Triassic origin can be interpreted to be displaced by the Cameros thrust during the Tertiary (Fig. 4).

Discussion

There is not a large difference in density between rocks from the basement and the sedimentary cover and in average (except for pyrite-rich units, relatively abundant in the filling of the Cameros Basin, Mata, 1997), they can be considered as equal, as shown in previous works that also used borehole data (borehole Castilfrío-1, Lanaja, 1987, Rivero et al., 1996). Small differences between the Cretaceous basin infill can account for the shape of some parts of the Bouguer anomaly curve. According to the data and the models proposed in this work, the Tertiary sedimentary wedge of the Rioja Trough is a significant source of gravimetric anomalies. Its lower density and the lower sedimentary thickness in the vicinity of the Cameros Basin (respect to the central part of the Ebro Basin) with respect to the average rock in the area explains the change in the Bouguer anomaly (Mezcua et al., 1996) (Fig. 5). In the Sierra de la Demanda, 30 km west of the studied transect, other gravimetric profiles (IGME database http://www.igme.es/internet/sigeof/inicio spa.html) indicate similar anomalies linked to the strong thickness of Tertiary deposits overthrusted by Paleozoic rocks. This allows for an interpretation of the relative maximum of the Bouguer anomaly in terms of a combination of near surface low-density sediments and crustal thickening towards the Iberian Chain (Salas and Casas, 1993; Guimerà et al., 2004; see Fig. 5). Previous interpretations of the position of the Iberian Moho in this area based on poorly constrained seismic reflection profiles (Pedreira, 2005; Pedreira et al., 2003, 2007) failed in noting that this kind of lateral heterogeneities can be responsible for the contradictory changes in thickness of the crust in the Ebro Basin with respect to the Iberian Chain. Northwards, crustal thinning in the Iberian Chain, together with the

Tertiary sedimentary wedge, explain the particular Bouguer anomaly in this part of the Iberian Peninsula.

To explain the observed magnetic anomaly, the presence of a high susceptibility/remanence body below the Oncala anticline is needed, since the magnetic remanence and susceptibility of Triassic to Cretaceous rocks cannot account for this high amplitude anomaly. To fit the observed profile, the susceptibility of the underlying rocks should be about $30\text{-}60\times10^{-3}$ (S.I. u.), a range of values that has only been found in igneous or metamorphic rocks. As it was mentioned above, volcanic rocks of mantelic origin are observed in this sector of the Iberian Range (Lago et al., 1988; Bastida et al., 1989), indicating a deep magmatic source and magma upwelling driven by large-scale basement faults. These rocks crop out as sills with a NW-SE orientarion (Lago et al., 1996). The age of this magmatic event is Late Triassic-pre-Hettangian, because these rocks appear within the shales and gypsum of the Upper Triassic (Keuper faces) and they are post-dated by the marine Jurassic carbonates. In our interpretation, we propose a dyke geometry for the rock volume responsible for the magnetic anomaly obtained. However, in spite of its higher density, and because of the relative small volume of the body, its contribution to the gravimetric anomaly is not significant.

Conclusions

In this work we show two new geophysical surveys across a NNE-SSW profile in the Cameros basin. Both the magnetic and gravimetric profiles show a positive anomaly in the central part of the studied area, although they do not overlap at the same position and are interpreted to have a different origin. With the aim of defining the relationship

between the structure and geometry of the rocks that constitutes the Cameros basin and the geophysical data, 2.5D modeling was applied.

The relative positive gravimetric anomaly can be produced by the difference in density between the Mesozoic and Paleozoic rocks which are denser than the surrounding rocks (the Tertiary molasse at both sides of the Cameros basin), combined with crustal thickening. To model the detailed profile and fit the field data a lower density must be used for the Lower Cretaceous units that crop out in the Oncala anticline.

The positive magnetic anomaly can be explained by the presence of a mafic body beneath the central part of the basin. The rocks that constitute this dyke are related to the sills that crop out in the northern basin border and the Moncayo area. This volcanic event would be pre-Hettangiense in age and would be related with the beginning of the rifting at western Tethys.

Acknowledgements

The authors thank Sylvia Gracia for her help in measuring with the KLY3S susceptibility meter. This study has been financed by the research projects CGL2009-08969 and CGL2009-10840 of the MICINN (Spanish Ministry of Science and Innovation). BOU acknowledges the “Juan de la Cierva Postdoctoral Program” from the MCINN.

References

Aranguren A., Cuevas J., Tubía J.M., Román-Berdiel T., Casas-Sainz A. and Casas-Ponsati A., 2003. Granite laccolith emplacement in the Iberian arc: AMS and gravity study of the La Tojiza pluton (NW Spain). J. Geol. Soc. London, 160, 435-445.

Arthaud F. and Matte P., 1975. Les décrochements tardi-herciniens du Sud-Ouest de l'Europe: Geómetrie et essai de reconstruction des conditions de la deformation. Tectonophysics, 25, 139-171.

Ayarza P. and Martínez-Catalán J.R., 2007. Potential field constraints on the deep structure of the Lugo gneiss dome (NW Spain). Tectonophysics, 439, 67-87.

Bastida J., Besteiro J., Reventos M.M., Lago M. and Pocovi, A., 1989. Los basaltos alcalinos subvolcánicos espilitizados de Arándiga (provincia de Zaragoza): estudio mineralógico y geoquímico. Acta Geol. Hisp., 24, 115-130.

Calvín P., Casas A.M. and Villalaín J.J., 2012. Origen de una anomalía magnética inversa en la unidad de Herrera (N de la Cordillera Ibérica). Geotemas, 13, 353.

Casas A., Keary P., Rivero L. and Adam C.R., 1997. Gravity anomaly map of the Pyrenean region and a comparison of the deep structure of the western and eastern Pyrenees. Earth Planet. Sci. Let., 150, 65-78.

Casas A.M., Cortés A.L. and Maestro A., 2000. Intra-plate deformation and basin formation during the Tertiary at the Northern Iberian Plate: origin and evolution of the Almazán Basin. Tectonics, 19, 762-786.

Casas A.M., Villalaín J.J., Soto R., Gil-Imaz A., Del Río P. and Fernández G., 2009. Multidisciplinary approach to an extensional syncline model for the Mesozoic

Cameros Basin (N Spain). Tectonophysics, 470, 3-20.

Casas-Sainz A.M., 1993. Oblique tectonic inversion and basement thrusting in the Cameros Massif (Northern Spain). Geodin. Acta , 6, 202-216.

Casas-Sainz A.M. and Gil-Imaz A., 1997. Extensional subsidence, contractional folding and thrust inversion of the Eastern Cameros Massif, northern Spain. Geol. Rundsch., 86, 802-818.

Casas-Sainz A.M., Casas A., Gapais D., Pérez A. and Tena S., 2000. Syn-tectonic sedimentation and thrust-and-fold kinematics at the intra-mountain Montalbán Basin (northern Iberian Chain, Spain). Geodin. Acta, 1, 1-17.

De Vicente G., Vegas R., Muñoz-Martín A., Van Wees J.D., Casas-Sainz A., Sopeña A., Sánchez-Moya Y., Arche A., López-Gómez J., Olaiz A. and Fernández-Lozano J., 2009. Oblique strain partitioning and transpression on an inverted rift: The Castilian Branch of the Iberian Chain. Tectonophysics, 470, 224-242.

De Vicente G. (ed.), 2004. Estructura alpina del antepaís ibérico. In: J.A. Vera (Ed.), Geología de España. S.G.E.-I.G.M.E., Spain.

Gómez-Ortiz D., Tejero-López R., Babin-Vich R. and Rivas-Ponce A., 2005. Crustal density structure in the Spanish Central System derived from gravity data analysis (Central Spain). Tectonophysics, 403, 131-149.

Guimerà J., Salas R., Vergés J. and Casas, A., 1996. Extensión mesozoica e inversión compresiva terciaria en la Cordillera Ibérica: aportaciones a partir del análisis de un perfil gravimétrico. Geogaceta, 20, 1691-1694.

Guimerà J., Mas R. and Alonso A., 2004. Intraplate deformation in the NW Iberian Chain: Mesozoic extension and Tertiary contractional inversion. J. Geol. Soc. London, 161, 291-303.

Guiraud M. and Séguret M., 1984. Releasing overstep model for the Late Jurassic-Early

Cretaceous (Wealdian) Soria strike-slip basin (North Spain), in: K. T. Biddle and N. Christie-Blick (Eds.), Strike-slip deformation, basin formation and sedimentation, S.E.P.M. Spec. Pub., 37, 159-175.

IGN, 2001. Anomalías Magnéticas de la Península Ibérica. Instituto Geográfico Nacional, Spain, 1 map.

Lago M., Pocovi A., Bastida J. and Amigó J.M., 1988. The alkaline magmatism in the Triassic-Liassic boundary of the Iberian Chain: geological and petrological characters. II Congreso Geológico de España, Granada, Comunicaciones, 2, 31-34.

Lago M., Pocovi A., Bastida J., Arranz E. and Gil-Imaz A., 1996. El vulcanismo alcalino, pre-Hettangiense, al NE de la Península Ibérica: puntos de interés para el Patrimonio Geológico. Geogaceta, 20, 1180-1182.

Lago M, Pocovi A, Bastida J. and Besteiro J., 1998. El magmatismo alcalino, del tránsito Trias-Lias inferior, en el área del Moncayo: Aspectos geológicos, petrológicos y geoquímicos. Turiaso, 9, 91-108.

Lanaja J.M., 1987. Contribución de la exploración petrolífera al conocimiento de la Geología de España. Inst. Geol. Min. España, Madrid, 465 p.

Lasanta C., Oliva B., Román-Berdiel T. and Casas A., 2011. When does AMS develop and register strain in extensional sedimentary basins? Geophysical Research Abstracts, 13, EGU2011-496.

Mata, P., 1997. Caracterización y evolución mineralógicas de la cuenca meosozica de Cameros (Soria, La Rioja). PhD Thesis, University of Zaragoza.

Mezcua J., Gil A. and Benarroch, R., 1996. Estudio gravimétrico de la Península Ibérica y Baleares, Inst. Geogr. Nac., Madrid, Spain, 2 maps.

Muñoz A., Soria A.R., Canudo J.I., Casas A.M., Gil A. and Mata, P., 1997.

Caracterización estratigráfica y sedimentológica del Albiense marino de la Sierra de Cameros. Implicaciones paleogeográficas. Cuadernos de Geología Ibérica, 22, 139-163.

Muñoz-Jiménez A. and Casas-Sainz A.M., 1997. The Rioja Trough (N Spain): tecto-sedimentary evolution of a symmetric foreland basin. Basin Research, 9, 65-85.

Pedreira D., 2005. Estructura cortical de la zona de transición entre los Pirineos y la Cordillera Cantábrica [CD-ROM], Ph.D. Thesis. Univ. de Oviedo, Spain, 343 pp.

Pedreira D., Pulgar J.A., Gallart J. and Díaz J., 2003. Seismic evidence of Alpine crustal thickening and wedging from the western Pyrenees to the Cantabrian Mountains (north Iberia). J. Geophys. Res., 108 (B4), 2204, doi:10.1029/2001JB001667.

Pedreira D., Pulgar J.A., Gallart J. and Torné M., 2007. Three-dimensional gravity and magnetic modeling of crustal indentation and wedging in the western Pyrenees-Cantabrian Mountains. J. Geophys. Res., 112, B12405, doi:10.1029/2007JB005021.

Pedrera A., Galindo-Zaldívar J., Tello and A. Marín-Lechado C., 2010. Intramontane basin development related to contractional and extensional structure interaction at the termination of a major sinistral fault: The Huércal-Overa Basin (Eastern Betic Cordillera). J. Geodyn., 49, 271-286.

Pinto V., Casas A., Rivero L. and Torné M., 2005. 3D gravity modeling of the Triassic salt diapirs of the Cubeta Alavesa (northern Spain). Tectonophysics, 405, 65-75.

Rey-Moral C., Gómez-Ortiz D. and Tejero-López R., 1999. Cálculo de la anomalía gravimétrica de una cuenca sedimentaria. Su aplicación en la cuenca de Almazán. Geogaceta, 25, 175-178.

Rey-Moral C., Gómez Ortiz D. and Tejero R., 2000. Spectral analysis and Gravity Modelling of the Almazán Basin (Central Spain). Rev. Soc. Geol. España, 13,

131-142.

Rey-Moral C., Gómez Ortiz D. and Tejero, R., 2003. Geometría del Moho en el centro peninsular obtenida a partir de datos gravimétricos. Boletín Geológico y Minero, 114, 41-56.

Rey-Moral C., Gómez-Ortiz D., Sánchez-Serrano F., Tejero-López R., 2004. Modelos de densidades de la corteza de la cuenca de Almazán (Provincia de Soria). Boletín Geológico y Minero, 115, 137-152.

Rivero L., Guimerà J. and Casas A., 1996. Estructura profunda de la cuenca de Cameros (Cordillera Ibérica) a partir de datos gravimétricos. Geogaceta, 20, 1695-1697.

Ruiz-Constán A., Stich D., Galindo-Zaldívar J. and Morales J., 2009. Is the northwestern Betic Cordillera mountain front active in the context of the convergent Eurasia-Africa plate boundary?. Terra Nova, 21, 352-359.

Salas R. and Casas A., 1993. Mesozoic extensional tectonics, stratigraphy and crustal evolution during the Alpine cycle of the eastern Iberian basin. Tectonophysics 228, 33-35.

Santolaria P., Casas A.M., Soto R. and Casas A., 2012. Análisis de las anomalías gravimétricas de la terminación suroccidental de la Unidad Surpirenaica Central. Geotemas, 13, 164.

Tischer G., 1966. El delta Weáldico de las montañas Ibéricas Occidentales y sus enlaces tectónicos. Not. Com. Inst. Geol. Min. España, 81, 53-78.

Villalaín J.J., Fernández-González G., Casas A.M. and Gil-Imaz A., 2003. Evidence of a Cretaceous remagnetization in the Cameros Basin (North Spain): implications for basin geometry. Tectonophysics, 377, 101-117.

Figure captions

Figure 1. Maps of the Bouguer (A) and magnetic (B) anomalies in the area. From Mezcua et al. (1996) and Instituto Geográfico Nacional (2001), respectively. (C) Geological setting of the studied area, showing the location of seismic profiles and cross-section of Fig. 2. Distribution of Triassic basalts following Lago et al. (1996) is also shown (D). E. Location of the study area in the Iberian Peninsula.

Figure 2. Seismic sections (courtesy of Repsol-exploración), and profiles (see location in Fig. 1.C) showing the gravimetric and magnetic anomalies obtained in the survey presented in this paper. Geological cross-section (constrained with surface data and seismic sections) showing the main structural features along the survey profile

Figure 3. Properties of the studied samples, corresponding to geological units of the studied sections. Magnetic susceptibility is given in $\times 10^{-6}$ S.I. units and density in gcm^{-3}.

Figure 4. 2.5D modeling of the residual anomalies with a simplified geometry of the basin. The physical properties considered for the geological bodies (labelled with numbers) are shown in table 1.

Figure 5. 2.5D modeling of the residual anomalies with a detailed geometry of the basin. The physical properties considered for the geological bodies (labelled with numbers) are shown in table 2.

Figure 6. Conceptual model proposed for the gravimetric and magnetic anomalies in the

western sector of the Ebro Basin. The physical properties considered for the geological bodies (labelled with numbers) are shown in table 2.

Table 1. Properties of the materials considered in the simplified 2.5D model (Fig. 4).

Table 2. Properties of the materials considered in the detailed 2.5D model (Fig.5).

Table 3. Properties of the materials considered in the proposed model for the gravimetric and magnetic anomalies in the western sector of the Ebro Basin (Fig. 6).

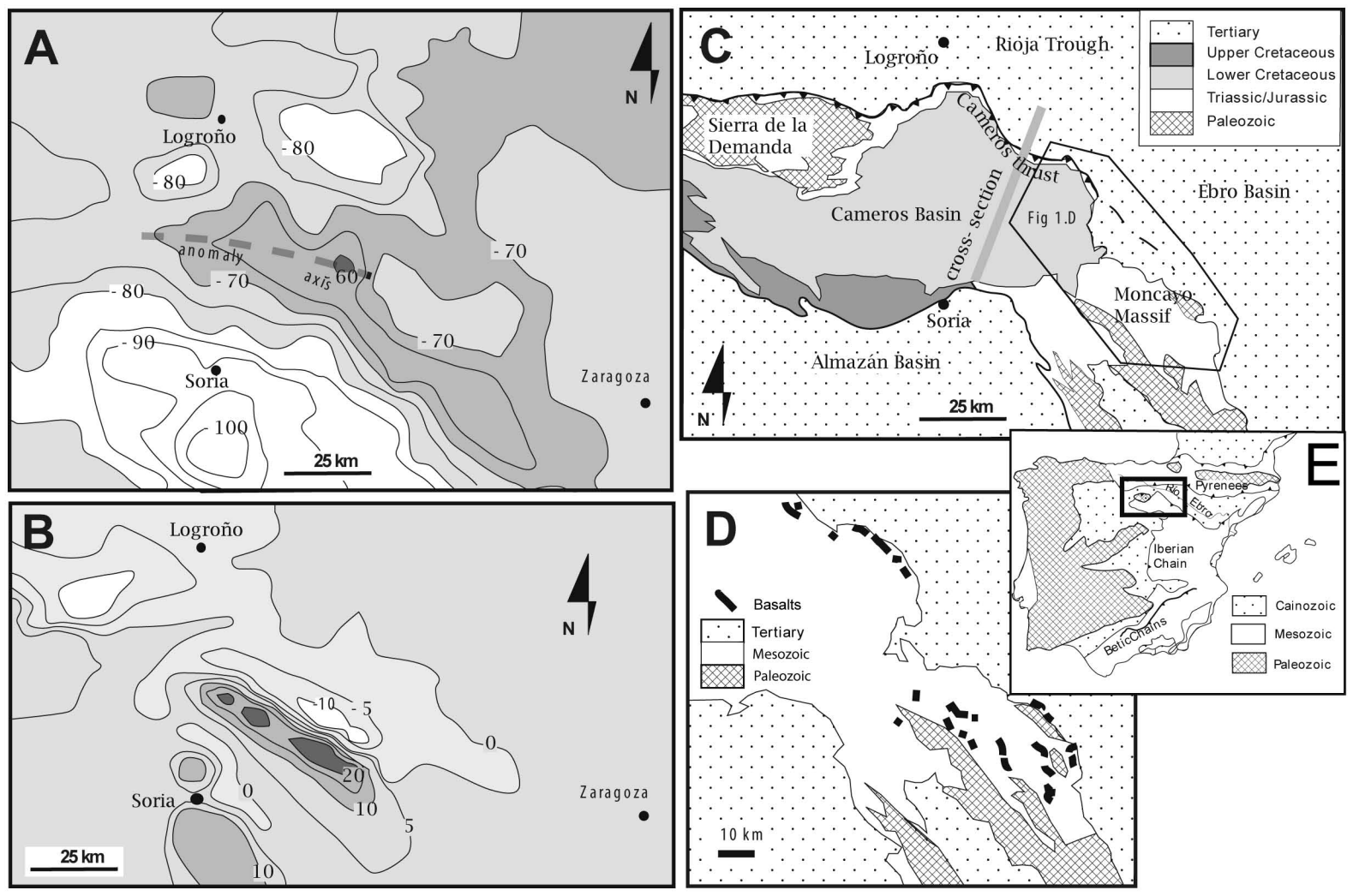
A
Logroño
Soria
Zaragoza
anomaly axis
-80
-70
-60
-90
-100
25 km
N
B
Logroño
Soria
Zaragoza
10
5
0
20
25 km
N
C
Logroño
Rioja Trough
Sierra de la Demanda
Cameros thrust
cross-section
Cameros Basin
Fig 1.D
Ebro Basin
Moncayo Massif
Soria
Almazán Basin
25 km
N
Tertiary
Upper Cretaceous
Lower Cretaceous
Triassic/Jurassic
Paleozoic
D
Basalts
Tertiary
Mesozoic
Paleozoic
10 km
E
Pyrenees
Rio Ebro
Iberian Chain
Betic Chains
Cainozoic
Mesozoic
Paleozoic

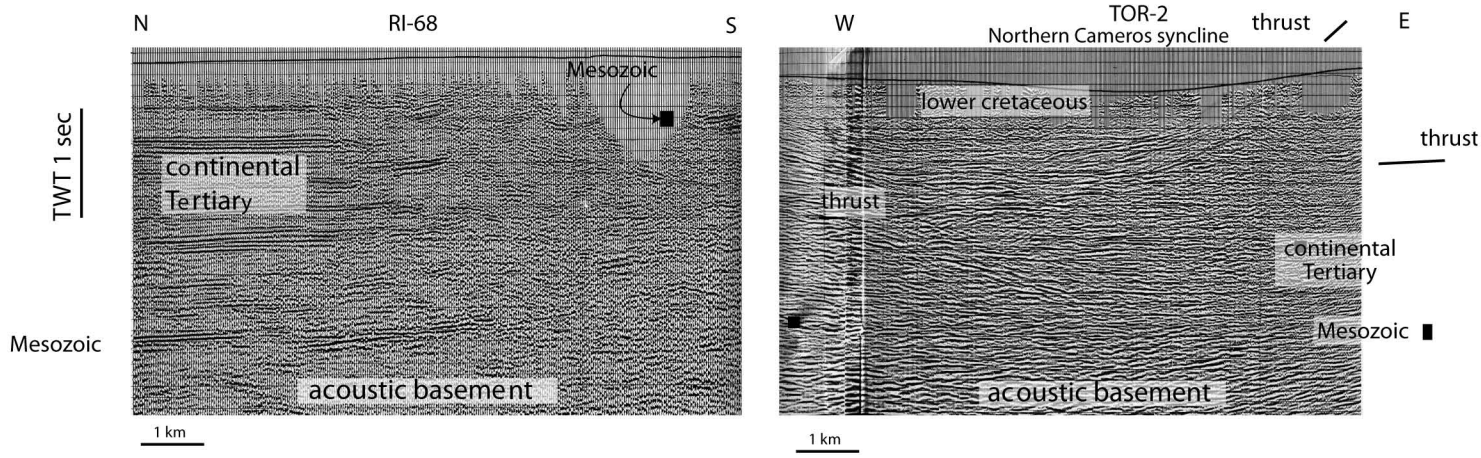
N
RI-68
S
W
TOR-2
Northern Cameros syncline
thrust
E
TWT 1 sec
Mesozoic
continental Tertiary
lower cretaceous
thrust
thrust
continental Tertiary
Mesozoic
Mesozoic
acoustic basement
acoustic basement
1 km
1 km

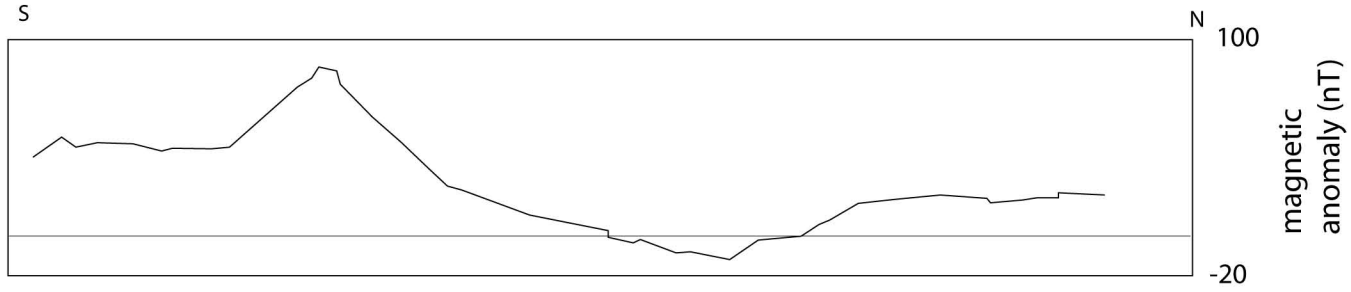
S
N
100
magnetic anomaly (nT)
-20

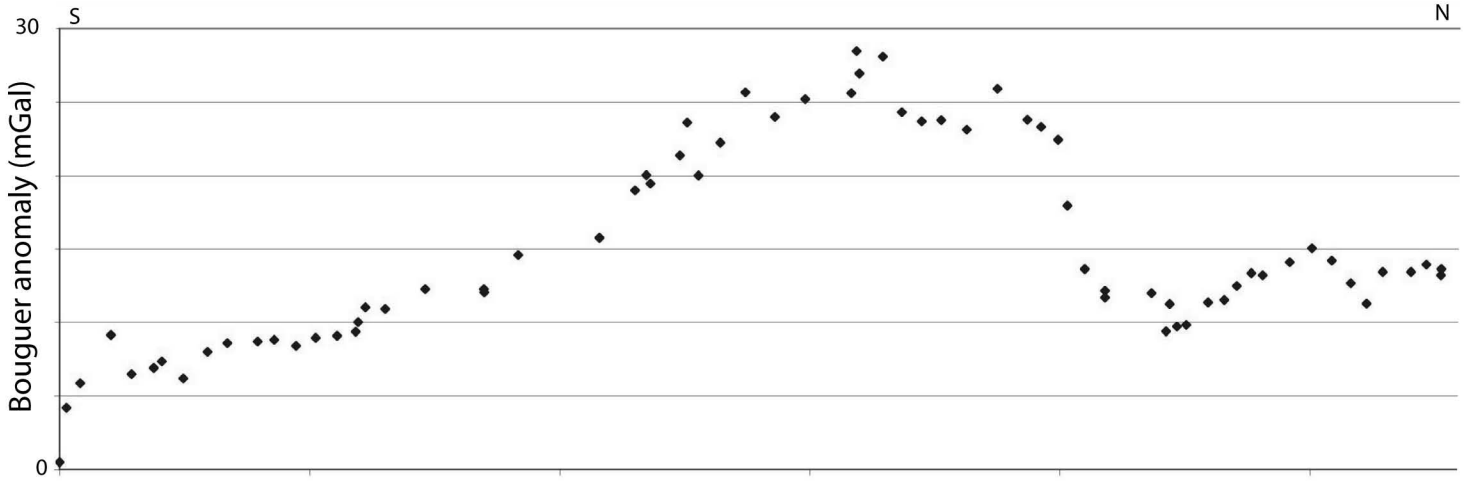
S
N
30
Bouguer anomaly (mGal)
0

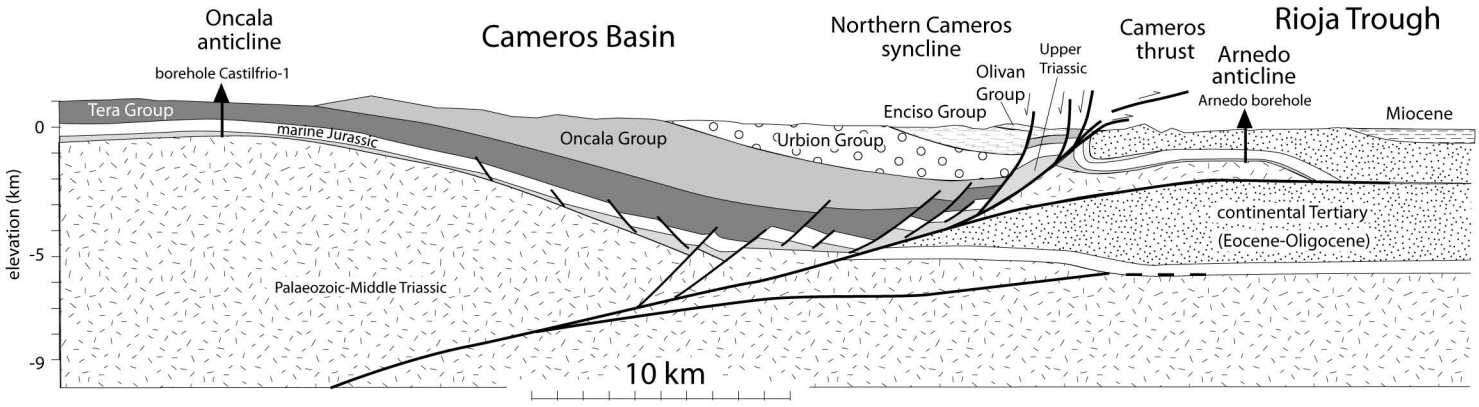
Oncala anticline
borehole Castilfrio-1
Cameros Basin
Northern Cameros syncline
Olivan Group
Upper Triassic
Cameros thrust
Arnedo anticline
Rioja Trough
Tera Group
Enciso Group
Arnedo borehole
Miocene
0
marine Jurassic
Oncala Group
Urbion Group
continental Tertiary (Eocene-Oligocene)
elevation (km)
-5
Palaeozoic-Middle Triassic
-9
10 km

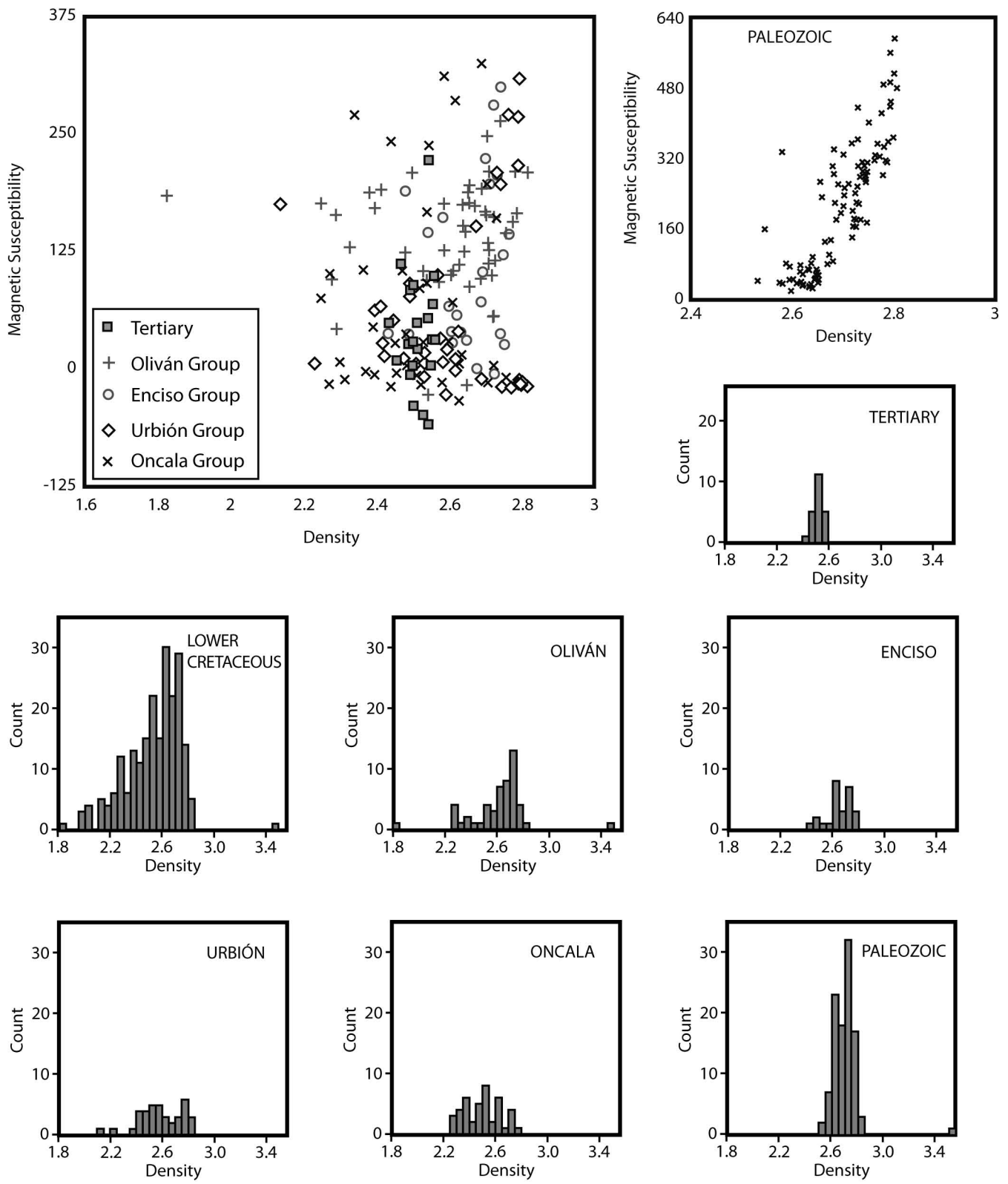
Magnetic Susceptibility
Density
Tertiary
Oliván Group
Enciso Group
Urbión Group
Oncala Group
PALEOZOIC
TERTIARY
LOWER CRETACEOUS
OLIVÁN
ENCISO
URBIÓN
ONCALA
PALEOZOIC
Count

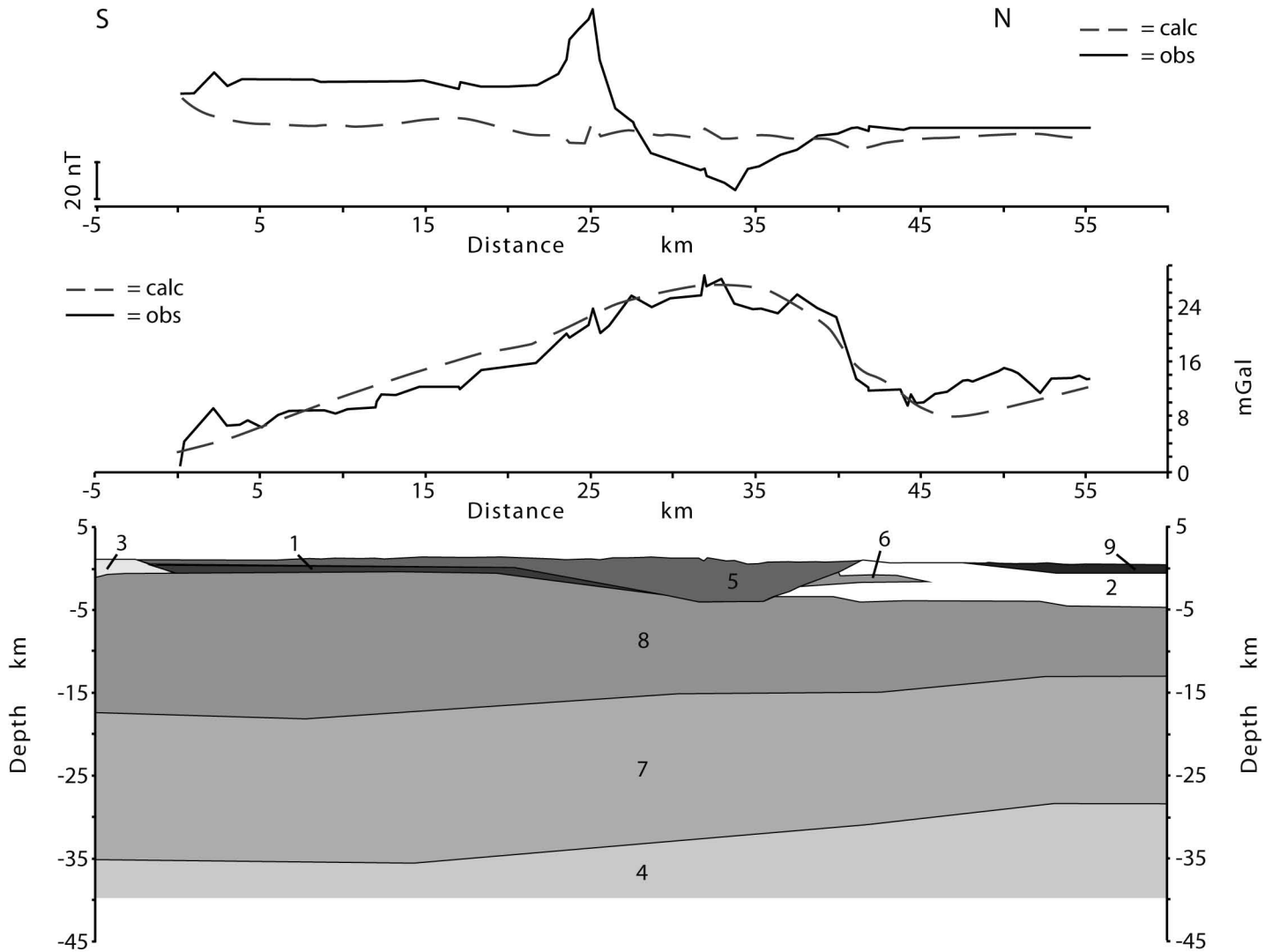
S
N
= calc
= obs
20 nT
-5
5
15
25
35
45
55
Distance
km
= calc
= obs
24
16
8
0
mGal
Depth
km
5
-5
-15
-25
-35
-45
1
2
3
4
5
6
7
8
9

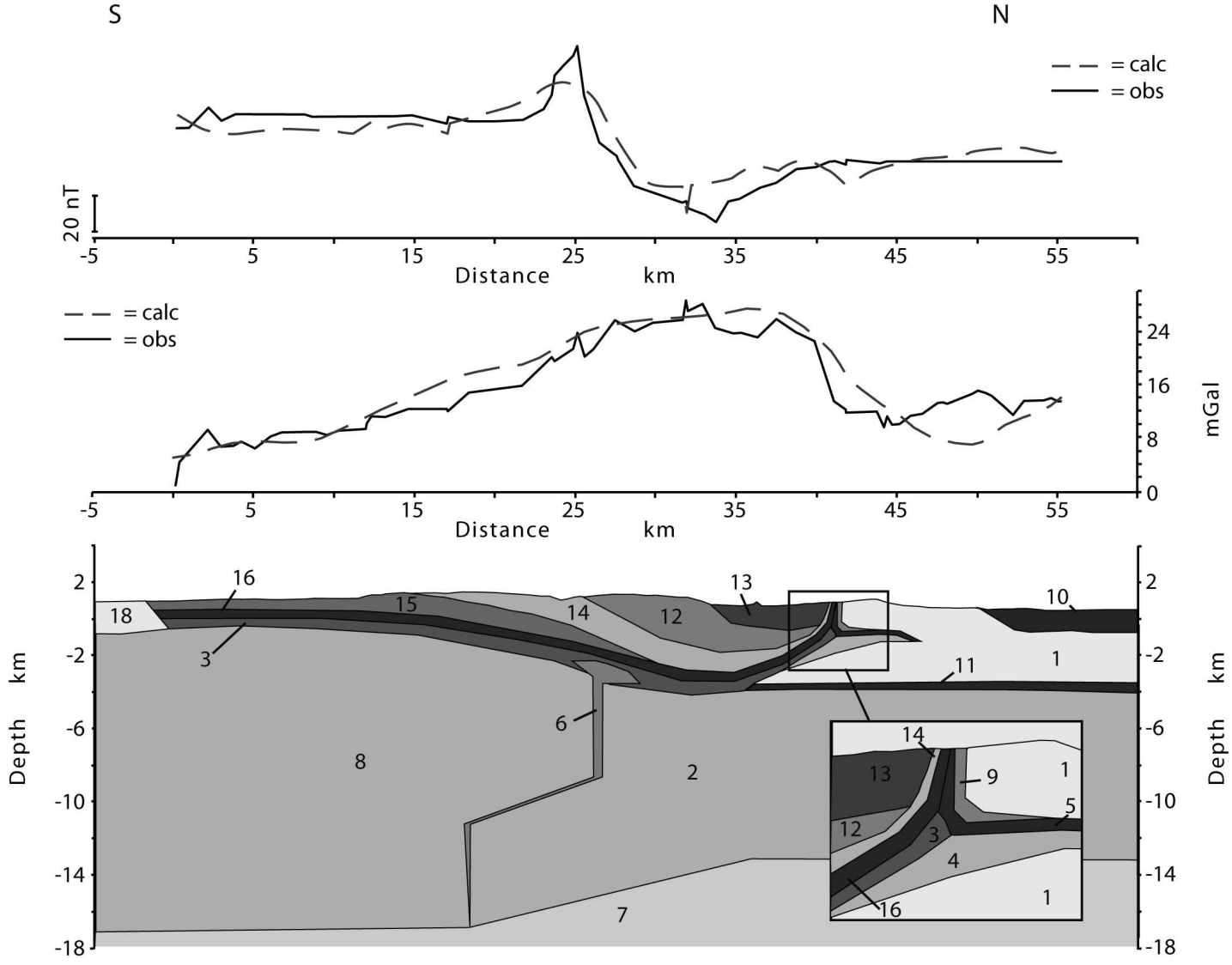
S
N
= calc
= obs
20 nT
-5
5
15
25
35
45
55
Distance
km
= calc
= obs
24
16
8
0
mGal
-5
5
15
25
35
45
55
Distance
km
Depth
km
2
-2
-6
-10
-14
-18
16
18
15
14
12
13
10
3
6
11
1
8
2
7
14
13
9
1
5
12
3
4
1
16

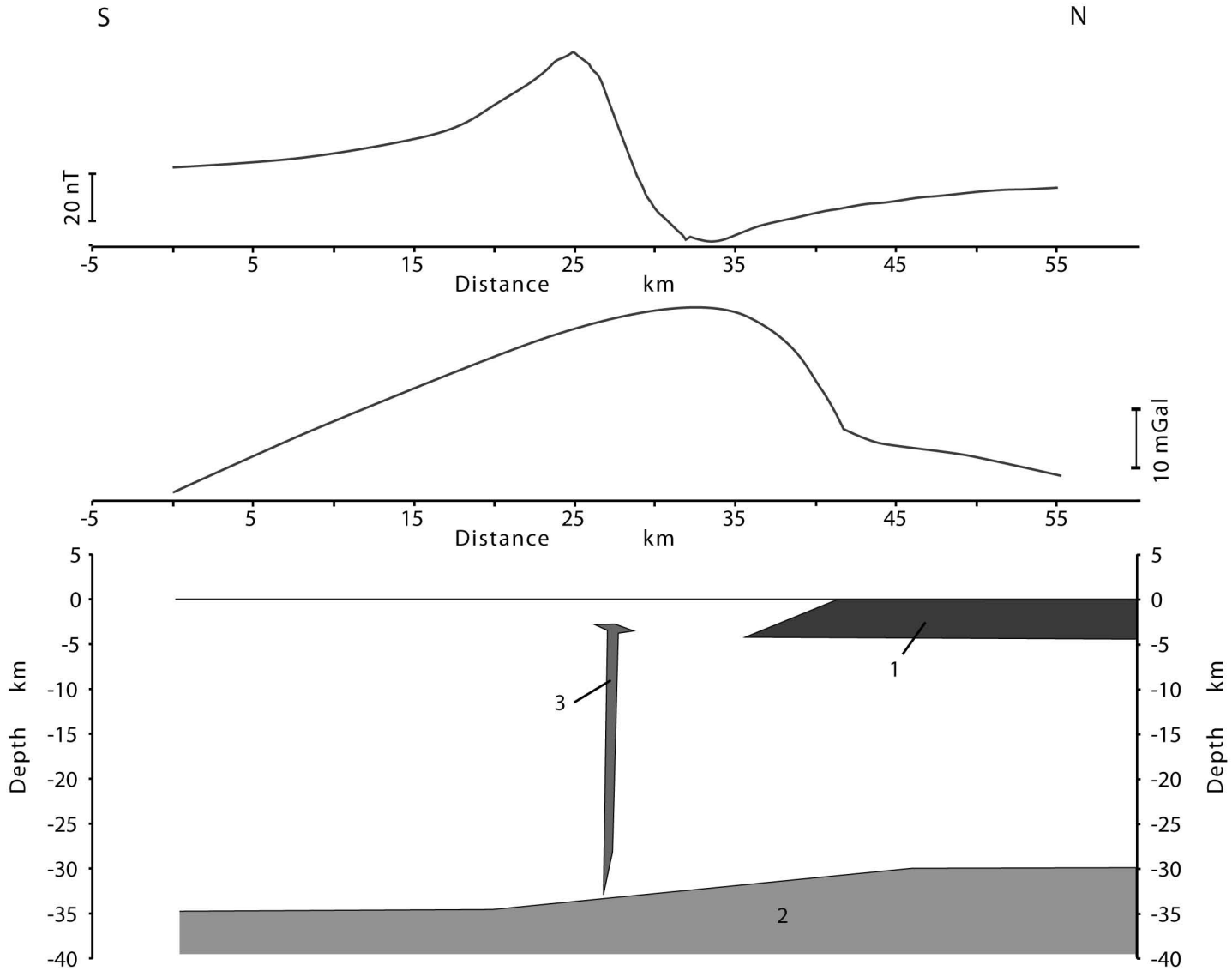
S
N
20 nT
-5
5
15
25
35
45
55
Distance
km
10 mGal
-5
5
15
25
35
45
55
Distance
km
5
0
-5
-10
-15
-20
-25
-30
-35
-40
Depth
km
1
2
3

Polygon Number	Group	Density (kgm^{-3})	Magnetic Susceptibility ($\times 10^{-6}$ S.I.)	Remanent Magnetization (A/m)	Remanent Declination	Remanent Inclination	Half Strike
1	Triassic	2550	4400	0.0000	0.00	15.00	100
2	Tertiary	2496	40	0.0000	0.00	0.00	100
3	Tertiary	2480	40	0.0000	0.00	0.00	100
4	Mantle	3350	0	0.0000	0.00	0.00	200
5	Cretaceous	2677	100	0.0211	0.00	56.00	100
6	Paleozoic	2660	200	0.0004	0.00	56.00	100
7	Lower Crust	2826	500	0.0000	0.00	0.00	100
8	Paleozoic	2689	200	0.0004	0.00	56.00	100
9	Miocene	2732	400	0.0000	0.00	0.00	100

Polygon Number	Group	Density (kgm^{-3})	Magnetic Susceptibility ($\times 10^{-6}$ S.I.)	Remanent Magnetization (A/m)	Remanent Declination	Remanent Inclination	Half Strike
1	Tertiary	2503	40	0.0000	0.00	0.00	100
2	Paleozoic	2700	200	0.0004	0.00	56.00	100
3	Triassic	2430	4400	0.0000	0.00	15.00	100
4	Paleozoic	2700	200	0.0004	0.00	56.00	100
5	Marine Jurassic	2750	300	0.0030	0.00	56.00	100
6	Dyke	2843	32200	0.0537	0.00	15.00	100
7	Lower Crust	2825	500	0.0000	0.00	0.00	100
8	Paleozoic	2700	200	0.0004	0.00	56.00	100
9	Albian	2650	0	0.0000	0.00	0.00	100
10	Miocene	2650	400	0.0000	0.00	0.00	100
11	Marine Jurassic	2750	300	0.0300	0.00	56.00	100
12	Urbión Group	2700	200	0.0250	0.00	90.00	100
13	Enciso Group	2790	200	0.0250	0.00	56.00	100
14	Oncala Group	2626	100	0.0093	0.00	56.00	100
15	Tera Group	2512	0	0.0250	0.00	56.00	100
16	Marine Jurassic	2750	200	0.0300	0.00	56.00	100
17	Mantle	2300	0	0.0000	0.00	0.00	100
18	Tertiary	2550	40	0.0000	0.00	0.00	100

Polygon Number	Group	Density (kgm^{-3})	Magnetic Susceptibility ($\times 10^{-6}$ S.I.)	Remanent Magnetization (A/m)	Remanent Declination	Remanent Inclination	Half Strike
1	Tertiary	2500	40	0.0000	0.00	0.00	100
2	Mantle	3300	0	0.0000	0.00	0.00	100
3	Dyke	2700	60000	0.0372	0.00	0.00	100